Soft Matter

Thermomechanical Properties of Monodomain Nematic Main-Chain Liquid Crystal Elastomers

Journal:	*Soft Matter*
Manuscript ID	SM-ART-06-2018-001178
Article Type:	Paper
Date Submitted by the Author:	08-Jun-2018
Complete List of Authors:	Merkel, Daniel; University of Wyoming College of Engineering and Applied Science, Mechanical Engineering Traugutt, Nicholas; University of Colorado at Denver , Mechanical Engineering VISVANATHAN, RAYSHAN; University of Colorado Boulder, Materials Science and Engineering Yakacki, Christopher; University of Colorado Denver, Mechanical Engineering Frick, Carl; University of Wyoming, Department of Mechanical Engineering

Submitted to: Soft Matter, June 2018

Thermomechanical Properties of Monodomain Nematic Main-Chain Liquid Crystal Elastomers

Daniel R. Merkel[1], Nicholas Traugutt[2], Rayshan Visvanathan[3], Christopher M. Yakacki[2], and Carl P. Frick[1λ]

[1] University of Wyoming, Department of Mechanical Engineering, Laramie, WY, USA

[2] University of Colorado Denver, Department of Mechanical Engineering, Denver, CO, USA

[3] University of Colorado Boulder, Materials Science and Engineering Program, Boulder, CO, USA

[λ] Corresponding author: Tel.: +1(307)766-2695; e-mail: cfrick@uwyo.edu

Abstract (100-150 words)

Two-stage thiol-acrylate Michael addition reactions have proven useful in programming main-chain liquid crystal elastomers (LCEs). However, the influence of excess acrylate concentration, which is critical to monodomain programming, has not previously been examined with respect to thermomechanical properties in these two-stage LCEs. Previous studies of thiol-acrylate LCEs have focused on polydomain LCEs and/or variation of thiol crosslinking monomers or linear thiol monomers. This study guides the design of monodomain LCE actuators using the two-stage methodology by varying the concentration of mesogenic acrylate monomers from 2 mol.% to 45 mol.% in stoichiometric excess of thiol. The findings demonstrate a technique to tailor the isotropic transition temperature by 44°C using identical starting monomers. In contrast to expectations, low amounts of excess acrylate showed excellent fixity (90.4 ± 2.9%), while high amounts of excess acrylate did not hinder actuation strain (87.3 ± 2.3%). Tensile stress-strain properties were influenced by excess acrylate. Linear

elastic behavior was observed parallel to the director with modulus increasing from 1.4 to 6.1 MPa. The soft elastic plateau was observed perpendicular to the director with initial modulus and threshold stresses increasing from 0.6 MPa to 2.6 MPa and 14 kPa to 208 kPa, respectively. Overall, this study examines the influence of excess acrylate on mechanical properties of LCE actuators.

1. Introduction

Liquid crystal elastomers (LCEs) are soft elastomeric networks comprised of mesogenic molecules, which give rise to a unique set of thermomechancial properties (Warner and Terentjev 2007; Dey et al. 2013). LCEs can be synthesized in the polydomain conformation in which mesogen alignment varies over the macroscopic scale, or in the monodomain conformation defined by a uniform director indicating the direction of mesogen alignment throughout the material. These arrangements generate isotropic and anisotropic mechanical properties, respectively, on the bulk scale. Inducing a liquid crystalline phase change under thermal (Kularatne et al. 2017), chemical (Boothby, Kim, and Ware 2017), electromagnetic (White 2018; Liu et al. 2017; M. Wang, Lin, and Yang 2016; M. Wang et al. 2016), or other stimulus disrupts the domain conformation through widespread mesogen reorganization to a highly disordered configuration designated as the isotropic phase. This phase transformation results in an associated change in mechanical properties. In the case of monodomain LCEs, the phase change causes a large, reversible change in sample dimensions, observed to be as high as 400% strain (Wermter and Finkelmann 2001). This phenomenon, known as two-way shape-memory, shape-switching, or shape-actuation, has been proposed for a variety of applications. Several recent reviews and investigative articles indicate applications for dynamic surfaces (Babakhanova et al. 2018; Torras et al. 2013), biomimetic materials (Prévôt, Ustunel, and Hegmann 2018; Gelebart et al. 2016; Schuhladen et al. 2014), cell scaffolds (Gao et al. 2016; Bera et al. 2015), soft robotics (Yuan et al. 2017), additive manufacturing (Ambulo et al. 2017; Kotikian et al. 2018), and optical coatings (Kragt, Broer, and Schenning 2018).

The mechanisms responsible for monodomain actuation and unique thermomechanical properties have been an emphasis of LCE research over the last 35 years. In particular, research has spotlighted the influences of chemical composition and structure on material response, which are outlined in recent reviews (Kularatne et al. 2017; White and Broer 2015). Yet the approach to synthesizing monodomain LCEs reliably and repeatably is not straightforward (Ohm, Brehmer, and Zentel 2010). Mesogen alignment techniques such as surface and photo-alignment produce excellent results (Kowalski, Guin, et al. 2017), offering unmatched spacial control of monodomain programming (Kowalski, Tondiglia, et al. 2017; Ware et al. 2016; Mostajeran, Ware, and White 2015; Ware et al. 2015); however, these techniques rely on the natural propagation of mesogen alignment through the reaction mixture and are consequently restricted to microstructures (Hessberger, Braun, and Zentel 2016; Urbanski et al. 2017; Fleischmann et al. 2013; Hong et al. 2009) or thin LCE films of about 100 μm or less. Alternatively, mechanical alignment techniques that are more suitable for bulk production of monodomain LCEs can be difficult to reproduce as the strategies are dependent on reliable reaction kinetics and adequate gelation before aligning forces can be applied (Donnio, Wermter, and Finkelmann 2000; Küpfer and Finkelmann 1991). Thiol-based chemical approaches have shown more repeatable results owing to selective reaction schemes (Yang et al. 2013; L. Wang et al. 2017).

Recently, Yakacki et al. introduced a highly reproducable two-stage thiol-acrylate Michael addition and photopolymerization procedure that has greatly increased the accessibility of LCEs to scientists and engineers (Yakacki et al. 2015). The approach uses off-the-shelf chemicals requiring no further modification and a simple one-pot reaction scheme. High conversion and repeatability result from the orthogonal nature of the initial thiol-acrylate Michael addition reaction and secondary photochemical acrylate homopolymerization (Hoyle and Bowman 2010; Nair et al. 2014); this is specifically advantageous for synthesizing monodomain LCEs at bulk scale with uniform director alignment and tunable thermomechanical properties. With appropriate chemical design, the initial reaction results in a polydomain LCE with reactive acrylates remaining in the elastomer. The monodomain can then be formed by mechanical elongation owing to a direct coupling between sample

extension and director orientation. Subsequent photopolymerization of the remaining acrylate fixes the configuration to a permament monodomain LCE capable of shape-actuation in response to thermal stimulus. Complex actuation can be achieved by non-uniform elongation prior to photopolymerization (Ahn, Liang, and Cai 2015). Additionally, the approach can be scaled up indefinitely, allowing facile synthesis of large quanties without loss of sample quality. This unique combination allows for unmatched control over director alignment in bulk monodomain LCEs. However, the monodomain cannot be fixed by a secondary reaction if there is no excess acrylate in the original mixture.

The selectivity of the initial thiol-acrylate reaction gives excellent control over the molecular structure of the LCE network, which can be designed to elicit specific thermomechanical properties. Crosslink density, mesogen concentration, and main-chain characteristics can be controlled by modulating relative concentrations and species of the constituent monomers. Previously, Saed et al. investigated the influence of crosslinker species and concentration on polydomain LCE properties (Saed, Torbati, et al. 2017) as well as the effects of spacing between mesogens (Saed, Volpe, et al. 2017). Exchangable bonding has also been achieved by designing excess thiol or other receptive moiety into the chemical formulation (Z. Wang et al. 2017; Hanzon et al. 2018; McBride et al. 2017; Pei et al. 2014). There have been a few studies on monodomain LCEs made by the thiol-acrylate and photopolymerization approach (Yakacki et al. 2015; Frick et al. 2016; Saed et al. 2016), however, the influence of excess acrylate concentration on thermomechanical and shape-actuation properties in LCEs of this type has not previously been explored.

This article investigates the influence of excess acrylate concentration on thermomechanical and actuation properties of monodomain nematic LCEs produced by the two-stage thiol-acrylate procedure. The reaction scheme requires some amount of excess acrylate to fix the monodomain conformation by the photochemical reaction; yet, the influence of varying excess acrylate content on monodomain fixity, thermomechanical properties, and actuation performance has not previously been explored. In this study, glass and isotropic

transition temperatures along with dynamic mechanical properties were investigated for compositions with up to 45 mol.% excess acrylate groups. Anisotropic mechanical properties were tested by quasistatic tensile tests with the liquid crystal director aligned parallel or perpendicular to the tensile axis. Shape-actuation strain and actuation rate resulting from the phase transition were investigated throughout the glassy, rubbery nematic, and isotropic thermal regimes. The results demonstrate a technique to tune the isotropic transition temperature, tensile properties, and actuation rate of LCE actuators without sacrificing mechanical properties or total actuation strain.

2. Materials and Methods

2.1. Materials

Monomers and the general fabrication procedure are shown in **Figure 1**. 4-bis-[4-(3-acryloyloxypropypropyloxy) benzoyloxy]-2-methylbenzene (CAS: 174063-87-7) (RM257) was purchased from Wilshire Technologies, Inc. (Princeton, NJ, USA). Pentaerythritol tetra (3-mercaptopropionate) (PETMP), 2,2-(ethylenedioxy) diethanethiol (EDDET), 2,6-di-tert-butyl-4-methylphenol (BHT), 2-hydroxy-4'-(2-hydroxyethoxy)-2-methylpropiophenone) (HHMP), dipropylamine (DPA), and toluene were purchased from Sigma-Aldrich, Inc. (St. Louis, MO, USA). All materials were used as-received without further purification.

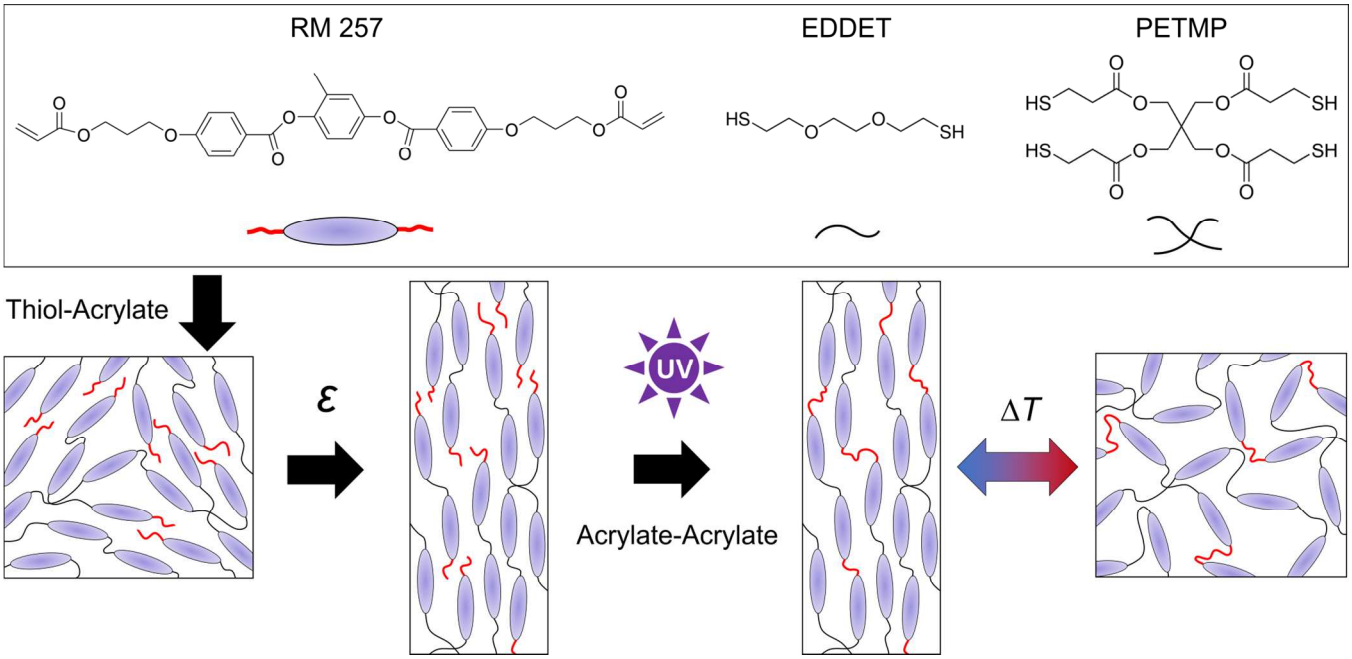

Figure 1: Monomers RM 257, EDDET, and PETMP polymerized via Michael addition, forming a polydomain elastomer with unreacted excess acrylate functional groups. The polydomain was elongated to form a monodomain, followed by photochemical reaction between the remaining acrylate groups. This programmed the monodomain and allowed reversible shape-actuation by heating/cooling through the isotropic transition temperature.

2.2. Liquid crystal elastomer fabrication

Main-chain liquid crystal elastomers were synthesized by a method adapted from a previous publication by one of the authors (Yakacki et al. 2015). The stoichiometry of the monomer mixture was systematically varied utilizing the concepts of thiol-acrylate click chemistry. The purpose was to produce tailored LCEs that contained between 0 and 45 mol.% excess acrylate functional groups (contributed by diacrylate mesogen RM 257) relative to thiol functional groups (contributed by tetrathiol PETMP and dithiol EDDET). The amount of crosslinker (PETMP) (10 mol.%) was calculated by the number of thiol functional groups contributed by the crosslinker relative to the total number of thiol groups contributed by the crosslinker and spacer (EDDET).

RM 257 and inhibitor BHT (200 ppm) were dissolved at 80°C in 30 wt.% toluene and mixed with EDDET and PETMP thiol monomers. Photo-initiator (HHMP) was added to the mixture (0.5 wt.%) and reheated to 80°C to dissolve. Catalyst (DPA) was diluted 1:50 by weight with toluene and mixed. The DPA/toluene solution was added to the reaction mixture (0.5 mol.%) to initiate a thiol-acrylate Michael addition reaction of equal parts thiol and acrylate functional groups. The solution was degassed under 21 in-Hg vacuum and cast between two glass slides with 1 mm polytetrafluoroethylene spacers between slides. The mixture polymerized overnight, forming a clear elastomer swollen with toluene. Toluene was extracted under 21 in-Hg vacuum at 80°C until the material reached a stable weight. Elastomers were opaque white at room temperature indicating a liquid crystalline phase in the polydomain conformation.

Monodomain LCEs were formed by uniaxial stretching to the strain at which the material transitioned from opaque white to optically transparent, often called the clearing strain. The monodomain could be programmed by photochemical reaction when excess acrylate was designed into the initial reaction mixture. Likewise, unstrained LCEs could be programmed in the opaque white polydomain. The photochemical reaction was initiated by exposure to 365 nm wavelength ultraviolet light (Blackray B-100A/R, UVP, Upland, CA, USA) for up to 1 hr. during which excess acrylate groups reacted to form new bonds in the network. Previous studies demonstrated high acrylate conversion within 10 minutes of starting the photochemical reaction in 2 mm thick LCEs (Yakacki et al. 2015) and 1 mm thick thiol-acrylate polymer networks with up to 100 mol.% excess acrylate (Nair et al. 2012). By comparison, the samples used in this study were 1 mm thick at most. This procedure had no apparent influence on LCEs that did not contain excess acrylate.

2.3. Fixity

Fixity (i.e., the relative length to which the monodomain was programmed) was quantitatively defined as the ratio of the fixed strain to the strain applied during the photopolymerization reaction (Equation 1). Polydomain LCEs were thermally cycled through the isotropic transition and measured at room temperature to obtain an initial length. The LCEs were then elongated to the monodomain, indicated by optical clearing of the material, and measured to obtain an applied strain ($\varepsilon_{applied}$). Elongated LCEs were held at the applied strain for the duration of the photochemical reaction to program the monodomain. The programmed samples were again thermally cycled through the isotropic transition then measured at room temperature to obtain the fixed strain (ε_{fixed}).

$$Fixity = \varepsilon_{fixed}/\varepsilon_{applied} \quad \text{(Eq. 1)}$$

2.4. Gel fraction

The degree of network formation in monodomain LCEs was evaluated by gel fraction (Equation 2). After photochemical reaction, LCEs were weighed to obtain an initial mass ($m_{initial}$). The LCEs were swelled in toluene at room temperature on a shaker table at 200 rpm until an equilibrium swollen mass was obtained. Toluene was extracted in a vacuum oven at 100°C and 21 in-Hg until an equilibrium final mass (m_{final}) was obtained. Gel fraction was calculated from the ratio of final mass to initial mass.

$$Gel\ fraction = m_{final}/m_{initial} \quad \text{(Eq. 2)}$$

2.5. Dynamic mechanical properties

Dynamic mechanical properties including storage modulus (*E'*) and loss tangent (*tan δ*) were investigated with a dynamic mechanical analyzer (DMA Q800, TA Instruments, New Castle, DE, USA) in DMA strain control mode using tensile grips. LCEs approximately 7 mm wide and 0.7 mm thick were clamped with 10 mm between grips, thermally cycled through the isotropic phase, cooled to sub-ambient temperature, and allowed to reach thermal equilibrium for 10 minutes prior to starting each test. All tests were performed at 0.2% strain amplitude, 0.01 N preload force, and 1 Hz oscillating frequency. Temperature was ramped up at 0.5°C/min to maintain uniform temperature through the thickness of each sample. Monodomain samples contracted in length with increasing temperature due to temperature dependence of nematic order and a phase transition at high temperature.

The glass transition temperature (T_g) was determined as the peak of the *tan δ* curve while the isotropic transition temperature (T_i) was taken as the minimum of the *E'* curve. A reduced temperature ($T_{reduced}$) was calculated such that thermal properties of the various LCE compositions tested in this study could be more easily compared with respect to the characteristic T_g and T_i of each composition. This was accomplished by requiring $T_{reduced} = 0$ at T_g and $T_{reduced} = 1$ at T_i for each composition. Thus, $T_{reduced}$ is defined by Equation 3. This approach is conceptually different than the reduced temperature commonly found in literature that investigated

phenomena near T_i. For example, see references (Krause et al. 2009; Sánchez-Ferrer and Finkelmann 2010; Giamberini et al. 2005) that use a simple normalization to T_i and reference (Petridis and Terentjev 2006) that normalizes to the temperature (T*) below which the isotropic phase is completely unstable.

$$T_{reduced} = (T - T_g)/(T_i - T_g) \quad \text{(Eq. 3)}$$

2.6. Tensile testing

Monodomain LCEs measuring 10 mm wide by 0.7 mm thick were clamped in the Q800 DMA with the liquid crystalline director aligned parallel to or perpendicular to the tensile axis. Samples were uniaxially extended in controlled strain mode at 6% strain/min. Engineering stress and strain were calculated using room temperature dimensions as the initial values. Tests were performed at a temperature corresponding to $T_{reduced}$ = 0.55 for each composition, which was an intermediate temperature within the nematic rubbery regime for each composition. This was chosen to demonstrate mechanical properties of the rubbery nematic regime without influence of the glass transition. Elastic modulus parallel to the director ($E_{\parallel}$) was evaluated as the slope of the loading curve at 10% strain. Elastic modulus perpendicular to the director ($E_{\perp}$) was evaluated as the slope of the loading curve at 1% strain. The threshold stress (σ_{th}) was taken as the maximum stress observed prior to formation of the stress plateau.

2.7. Actuation

Shape-actuation was evaluated in DMA controlled force mode with zero bias stress using tensile grips. LCEs were clamped with the director aligned to the strain axis, cooled to -25°C, and allowed to thermally equilibrate for 10 minutes prior to starting each test. A 0 N preload force was maintained while the samples were heated at 0.5°C/min until an equilibrium isotropic length was obtained before cooling at the same rate to the equilibrium nematic length. Sample length was measured throughout the test. Engineering strain was calculated by normalizing sample length to the equilibrium isotropic sample length, which was the shortest observed length for each sample.

2.8. Wide-angle X-ray scattering

In-situ wide-angle X-ray scattering (WAXS) experiments were performed using a Forvis Technologies X-ray instrument. The instrument was equipped with a 30 W Genix 3D X-ray generator with a copper anode (wavelength = 1.5405 Å and energy = 8.05092 keV) and Dectris Eiger R 1M detector with pixel size of 75 x75 μm^2. A flux of 4 x 10^7 X-ray photons/s was achieved with a beam size of 0.8 x 0.8 mm^2 at the sample position. All measurements were taken in transmission mode at temperatures equivalent to $T_{reduced}$ = 0.5 and $T_{reduced}$ = 1.25 corresponding to the nematic and isotropic thermal regimes for each composition. The 0 mol.% excess sample was strained by hand until optically clear to achieve a temporary monodomain and verify a nematic structure at 31°C. The remaining samples were tested without any applied strain or constraints.

3. Results

3.1. Liquid crystal elastomer fabrication and fixity

Monodomain nematic main-chain LCEs were fabricated using a the two-stage chemical reaction consisting of an initial thiol-acrylate base-catalyzed Michael addition reaction followed by a secondary photochemical radical reaction between remaining acrylate groups. For the first-stage reaction, thiol-acrylate stoichiometry was adjusted to produce polydomain LCEs with up to 45 mol.% excess unreacted acrylate functional groups relative to thiol groups after the initial Michael addition reaction. Further increasing the acrylate content produced LCEs of poor constitution that were easily damaged during manual handling. Thus, compositions with greater than 45 mol.% excess acrylate were not studied. The chemical composition, which was made up of mesogenic diacrylates (RM 257), flexible dithiol spacers (EDDET), and flexible tetrathiol crosslinkers (PETMP), assembled into a network of mesogens and spacers composing a main-chain with few crosslinks throughout the network. Reaction mixtures with 0 mol.% excess acrylate (*i.e.* stoichiometric balance of thiol and acrylate groups) formed polydomain LCEs with no unreacted acrylate groups remaining after the initial Michael addition reaction, and consequently were not receptive to the subsequent photochemical reaction. Increasing the

acrylate content resulted in an equivalent increase in mesogen concentration with concurrent decrease in spacer concentration (**Figure 2**). Crosslinker concentration remained relatively constant between compositions, although a slight decrease was observed with increased acrylate. The effect of increasing the acrylate concentration from 0 mol.% to 45 mol.% excess acrylate relative to the total thiol corresponded to a decrease in crosslinker concentration from 2.6 mol.% to 2.1 mol.% crosslinker relative to the LCE network, decrease in spacer concentration of 46.6 mol.% to 37.9 mol.%, and an increase in mesogen concentration from 50.8 mol.% to 60.0 mol.%. Thus, the effect of variation in crosslinker concentration on network properties was expected to be negligible compared to the influences of varied spacer and mesogen concentrations.

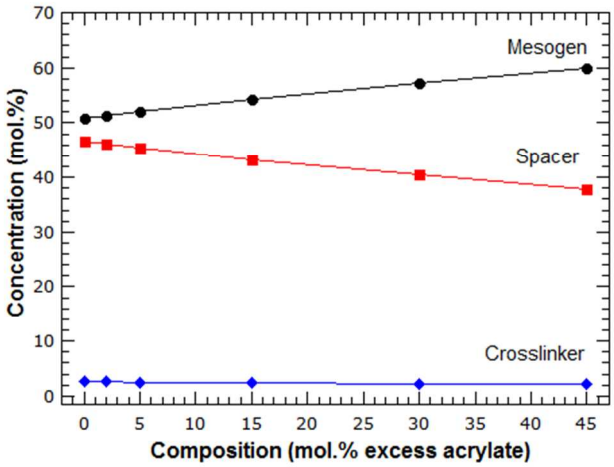

Figure 2: Monomer concentrations relative the total network compositions. Increase in diacrylate mesogen resulted in a proportional decrease in spacer concentration with negligible change in crosslinker concentration.

Prior to the secondary reaction, the monodomain was formed by elongating polydomain LCEs with unreacted acrylate groups to an applied mechanical strain that was just beyond optical clearing of the sample (**Figure 3a**). The presence of unreacted acrylate groups after Michael addition strongly influenced the mechanical viability of the polymerized networks and limited the concentration of acrylate allowable in the chemical formulation. Applied strain to observe clearing varied between compositions from 85% strain for the 2 mol.% composition to 128% for the 45 mol.% composition. LCEs with acrylate content greater than 45 mol.% in excess of thiol ruptured before completing the polydomain-monodomain transition and were unsuitable for this study. The

applied strain was held constant during the subsequent photochemical reaction between remaining acrylate groups, which formed new network links and changed the equilibrium state of the LCE.

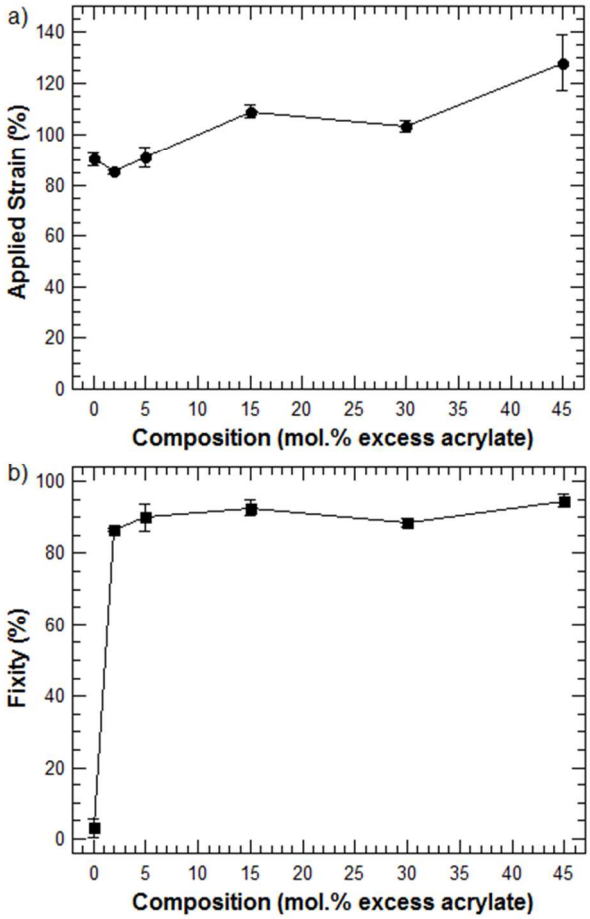

Figure 3: (a) After Michael addition, strain was applied to the clearing point of the LCEs for subsequent photochemical reaction of the remaining acrylate groups to program the monodomain. (b) All compositions with excess acrylate achieved monodomain fixity (Eq. 1) greater than 85% after the secondary reaction.

All compositions with excess acrylate achieved over 85% fixity after the photochemical reaction (**Figure 3b**), demonstrating efficient programming of the monodomain even with low concentration of excess acrylate. As expected, fixity of the 0 mol.% excess acrylate composition was near zero and the polydomain resumed after thermal cycling through the isotropic phase. Gel fraction varied between 92% and 97% for all compositions

after photochemical reaction indicating efficient network formation with low soluble content (**Supplementary Figure 1**). This was comparable to a previous study (Yakacki et al. 2015).

3.2. Transition temperatures and dynamic mechanical properties

Experimental measurements of *tan δ* and *E'* were used to define T_g and T_i, respectively (**Figure 4**). T_g was similar for low excess acrylate compositions (0 mol.%, 2 mol.%, and 5 mol.%) and increased from 2°C to 14°C as excess acrylate increased to 45 mol.%. T_i increased more dramatically with acrylate content, broadening the rubbery nematic range. The 0 mol.% composition demonstrated the lowest T_i at 58°C, which increased to 113°C for the 45 mol.% composition. Accordingly, the breadth of nematic rubber region broadened from 55°C to 99°C as excess acrylate increased from 0 mol.% to 45 mol.%.

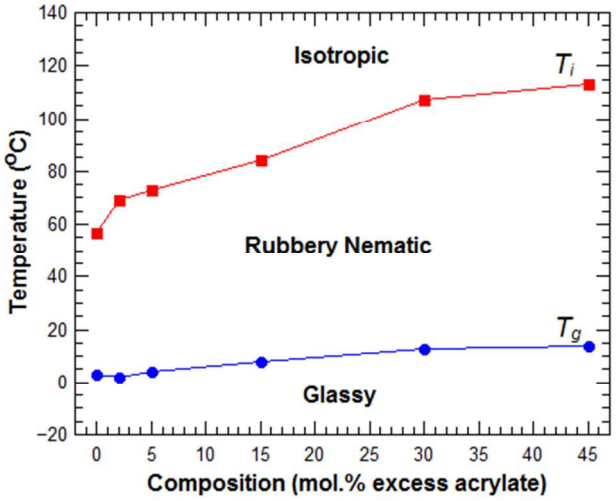

Figure 4: Increasing acrylate content resulted in disproportionate increases of glass and isotropic transition temperature, which effectively broadened the rubbery nematic regime.

Representative *E'* and *tan δ* curves for each composition are shown in **Figure 5a** using $T_{reduced}$ for the horizontal axis, calculated by Equation 3 for each composition. $T_{reduced} = 0$ corresponds to T_g and $T_{reduced} = 1$ corresponds to T_i for each composition. This normalization caused the glassy, rubbery nematic, and isotropic regimes to overlay one-another, simplifying comparisons between compositions. Dynamic mechanical properties relative

to a true temperature scale are shown in **Supplementary Figure 2a**. In general, monodomain compositions did not demonstrate significant variation in *E'* in each regime except for a distinct trend at T_i. The *E'* in the glassy plateau was 10^3-10^4 MPa for all compositions. Heating beyond T_g caused several orders of magnitude decrease in *E'* into the rubbery nematic regime, reaching a magnitude of 2-3 MPa for the monodomain compositions. *E'* decreased dramatically at T_i due to dynamic soft elasticity. The magnitude of *E'* and the sharpness of the dip was strongly dependent on composition. Low acrylate compositions demonstrated acute dips at T_i with the lowest magnitude of *E'* reaching 0.2 MPa for the 2 mol.% composition. Higher acrylate compositions showed less acute *E'* dips with a maximum of 1.1 MPa for the 45 mol.% composition. Further heating beyond T_i caused *E'* to increase continuously and resume similar magnitude for all monodomain compositions. *E'* of the polydomain 0 mol.% composition was significantly less than the monodomain compositions over all thermal regimes (**Figure 6a**).

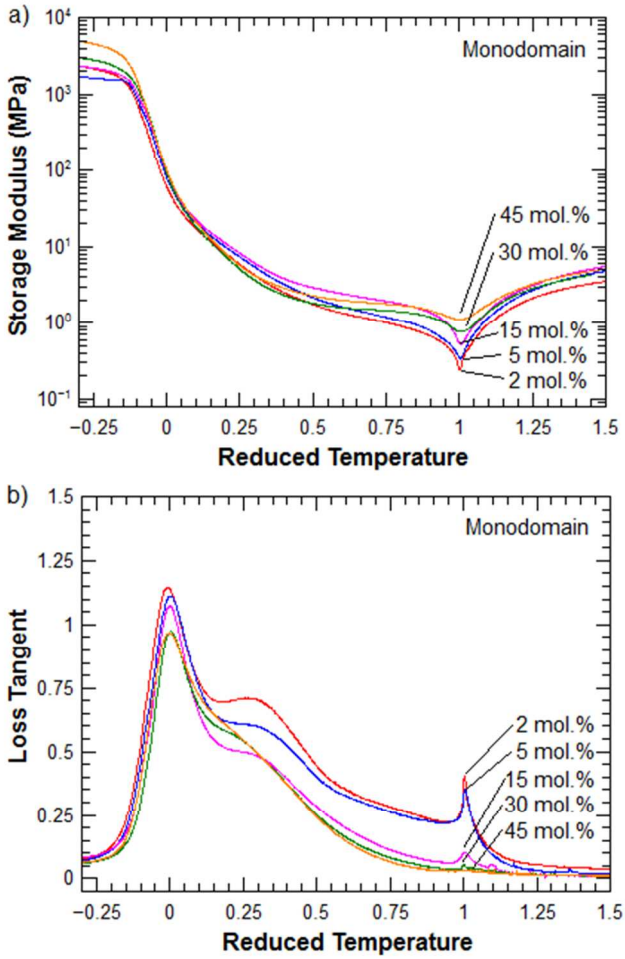

Figure 5: (a) Storage modulus of monodomain compositions did not vary significantly with changes to composition, except for the softening at the isotropic transition ($T_{reduced}$ = 1). (b) Damping properties were significant throughout the rubbery nematic regime (0 < $T_{reduced}$ < 1) for low acrylate monodomain LCEs. High acrylate LCEs (15 – 45 mol%) demonstrated significant damping only in vicinity of the glass transition ($T_{reduced}$ = 0). A reduced temperature scale normalized to the glass and isotropic transition temperatures simplified comparison of glassy, rubbery nematic, and isotropic regimes.

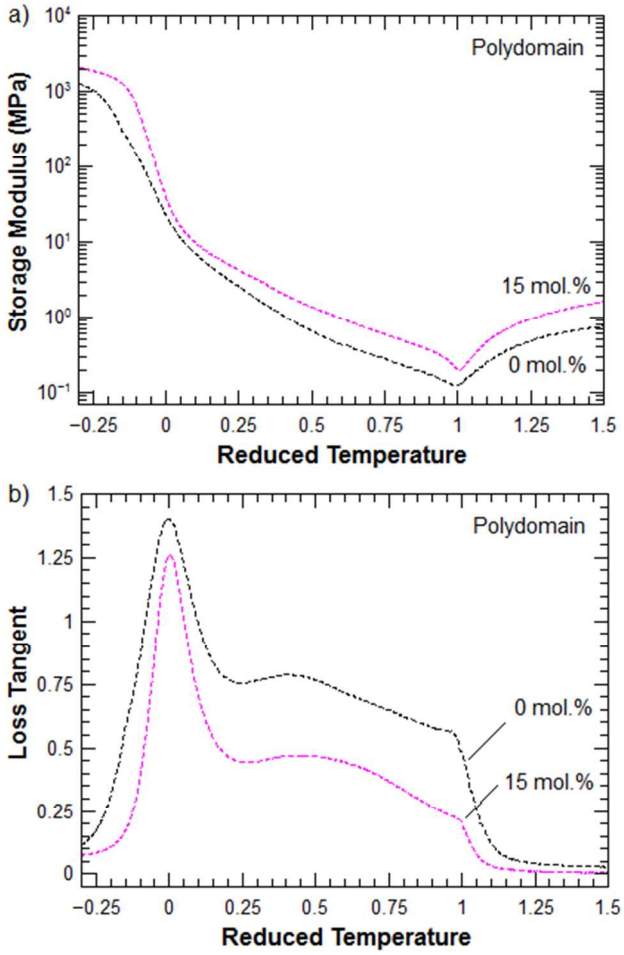

Figure 6: (a) Storage modulus of polydomain compositions. (b) Damping properties were significant throughout the rubbery nematic regime (0 < $T_{reduced}$ < 1). A reduced temperature scale normalized to the glass and isotropic transition temperatures simplified comparison of glassy, rubbery nematic, and isotropic regimes.

To better illustrate the influence of mesogen alignment, a 15 mol.% excess acrylate composition was photopolymerized in the polydomain conformation. The 15 mol.% excess acrylate polydomain demonstrated a T_g of 12°C, 4° higher than that of the 15 mol.% monodomain and showed no change in T_i. Nominal values for *E'* in the glassy regime were similar for both materials indicating that mesogen alignment had little influence (**Figure 6a**). Heating the polydomain into the rubbery nematic regime caused a continuous decrease in *E'* until T_i was reached, whereas the monodomain approached a plateau in *E'* above $T_{reduced}$ = 0.5. *E'* of the polydomain was approximately 1.5 orders of magnitude less than that of the monodomain near T_i, demonstrating a significant influence of mesogen alignment in the rubbery nematic range. The dip in *E'* at T_i reached a minimum of 0.2 MPa for the polydomain compared to 0.5 MPa for the monodomain. Further heating into the isotropic regime caused *E'* to increase continuously; however, *E'* of the polydomain remained approximately 2.5 MPa less than that of the monodomain. A direct comparison between dynamic properties of polydomain and monodomain is shown in **Supplementary Figure 2b**. Dimensional change as the samples entered the isotropic state were not considered when calculating *E'*; however, a large increase in cross-sectional area consistent with phase transition of the monodomain sample would indicate a decrease in *E'* compared to the polydomain sample that exhibited a negligible shape change when heated into the isotropic regime. This is in contrast to the *E'* observations indicating that the result is not in error due to the measurement technique.

Tan δ of monodomain compositions demonstrated maximum damping properties at T_g and a decay in magnitude with further heating that was strongly dependent on composition (**Figure 5b**). In general, low acrylate compositions showed greater damping throughout the rubbery nematic regime, maintaining elevated magnitude up to T_i. At T_g, maximum *tan δ* was highest for the 2 mol.% composition at 1.15 and decreased to 0.97 for both the 30 mol.% and 45 mol.% compositions. At temperatures beyond T_g, monodomain compositions demonstrated secondary peaks, shoulders, or continuous decay depending on composition. A secondary peak of magnitude 0.71 developed in the 2 mol.% composition while the 5 mol.% composition demonstrated a prominent shoulder of magnitude 0.61 at $T_{reduced}$ = 0.3. Both compositions assumed similar magnitudes with

further heating, approaching equal magnitudes of 0.22 at temperature just below T_i. The 15 mol.% and 30 mol.% compositions also developed shoulders of magnitude 0.51 and 0.57, respectively at $T_{reduced}$ = 0.2 while the 45 mol.% compositions demonstrated a continuous decay from the T_g peak. The three high acrylate compositions approached similar magnitude at $T_{reduced}$ = 0.3 and decayed uniformly to near-zero magnitude just below T_i. *Tan δ* peaks developed at T_i with peak magnitude dependent on composition, reaching a maximum 0.41 for the 2 mol.% composition and a minimum of 0.05 for the 30 mol.% composition. No peak was detectable for the 45 mol.% composition.

The 0 mol.% polydomain composition demonstrated significantly greater *tan δ* compared to the monodomain compositions, reaching peak magnitude of 1.40 at T_g (**Figure 6b**). *Tan δ* remained elevated throughout the rubber nematic regime, reaching a secondary peak of magnitude 0.79 at $T_{reduced}$ = 0.4, and a minimum of 0.56 at T_i. Further increase in temperature beyond T_i returned *tan δ* to near zero magnitude for all compositions. *Tan δ* of a 15 mol.% excess acrylate polydomain LCE showed improved damping characteristics over the monodomain of the same composition (**Supplementary Figure 2b**). The prominent peak at T_g reached 1.26 compared to 1.07 for the monodomain. *Tan δ* maintained magnitude greater than 0.2 throughout the rubbery nematic regime, producing a secondary maximum of 0.47 at $T_{reduced}$ = 0.5 before an abrupt decrease toward zero at the isotropic transition.

3.3. Tensile testing

When loaded monotonically in tension at $T_{reduced}$ = 0.55, rubbery nematic monodomain LCEs demonstrated traditional elastomeric response parallel to the director with $E_{\parallel}$ influenced by composition (**Figure 7a**). Low acrylate 2 mol.% and 5 mol.% compositions exhibited comparable $E_{\parallel}$ of about 1.4 MPa. Increasing acrylate content to 15 mol.% and 30 mol.% increased $E_{\parallel}$ to 2.3 MPa. The 45 mol.% composition demonstrated the highest $E_{\parallel}$ of 6.1 MPa. Deformation parallel to the director did not produce necking (**Figure 7b**). Perpendicular to the director, LCEs demonstrated an initial elastic region and threshold stress associated with a soft elastic

stress plateau followed by a final elastic region (**Figure 7c**). $E_{\perp}$ of the initial elastic region and σ_{th} marking the onset of widespread mesogen rotation increased with excess acrylate from 0.6 MPa to 2.6 MPa and from 14 kPa to 208 kPa, respectively, as excess acrylate content increased from 2 mol.% to 45 mol.%. The onset of mesogen rotation resulted in necking, which spread through the gauge length (**Figure 7d**).

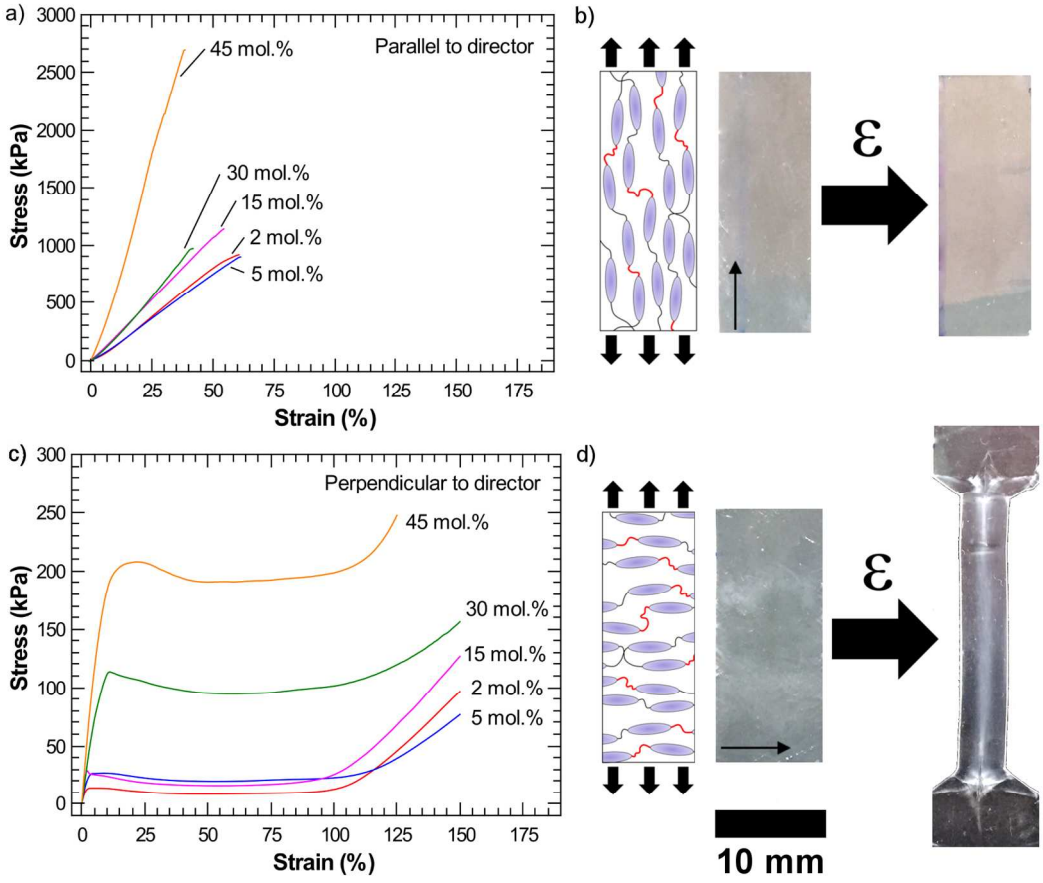

Figure 7: (a) Tensile modulus parallel to the director ($E_{\parallel}$) of monodomain LCEs increased with acrylate content. (b) LCE before (left) and after (right) tensile loading along the director demonstrating elastic recovery. (c) Tensile modulus perpendicular to the director ($E_{\perp}$) and threshold stress (σ_{th}) of monodomain LCEs increased with acrylate content. (d) LCE before (left) and after (right) tensile loading perpendicular to the original director demonstrating residual deformation due to mesogen reorientation. Small arrow indicates initial director orientation.

3.4. Actuation

Monodomain LCEs demonstrated large contraction along the liquid crystalline director when heated into the isotropic regime and extension upon cooling back to the nematic regime (**Figure 8a**). No mechanical bias was necessary to produce actuation. Sample dimensions were stable below T_g. Heating through the rubbery nematic regime induced dimensional contraction along the liquid crystalline director with concurrent expansion in width and thickness. The total actuation strain did not depend strongly on acrylate content and ranged from 84% actuation strain for the 15 mol.% composition to 90% actuation strain for the 45 mol% composition. The rate of actuation in the rubbery nematic regime did not vary significantly between compositions; however, near T_i, actuation rate was dependent on composition with low acrylate concentration producing higher change in strain per degree Celsius compared to high acrylate compositions (**Figure 8b**). Although actuation rates observed during heating and cooling were similar for each composition, actuation rate during cooling was repeatedly higher and is reported here. The 2 mol.% composition produced the highest actuation rate of 10.8% strain/°C during cooling and the 30 mol.% and 45 mol.% composition showed the lowest actuation rate of 1.8%/°C. Low excess acrylate compositions (2 mol.%, 5 mol.%, and 15 mol.%) did not shown significant strain actuation after heating beyond T_i; however, the high excess acrylate compositions continued to contract well into the isotropic regime.

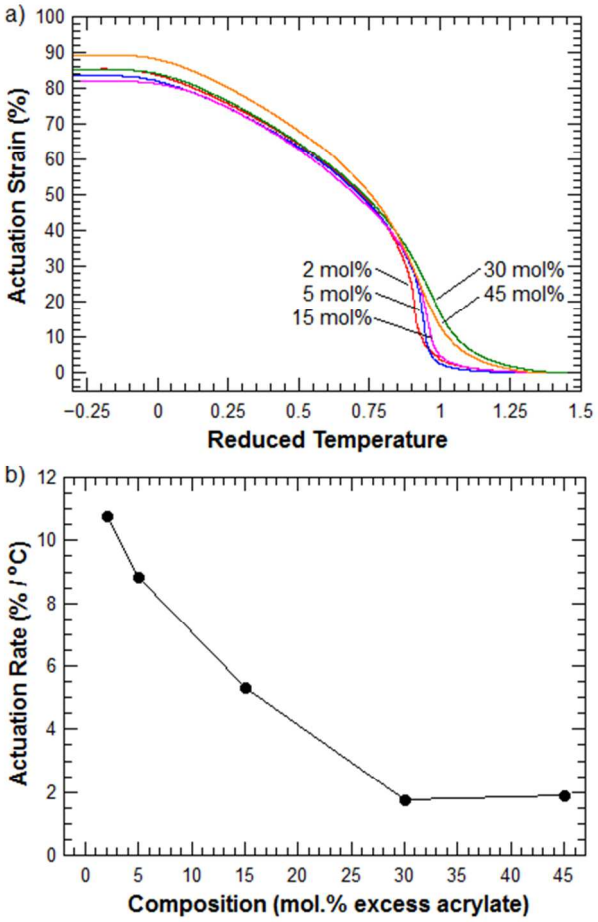

Figure 8: (a) LCE expansion upon cooling from the isotropic regime ($T_{reduced} > 1$) to the rubbery nematic regime ($T_{reduced} < 1$). All compositions demonstrated comparable total actuation strain. High acrylate compositions actuated significantly in the isotropic regime while low acrylate compositions demonstrated negligible actuation in the isotropic regime. (b) Maximum actuation rate near the isotropic transition ($T_{reduced} = 1$) decreased against acrylate content.

The actuation stroke observed during heating (not shown) did not overlap the stroke observed during cooling and is attributed to thermal lag despite the use of slow heating/cooling rate of 0.5°C/min. A residual loss in sample length of less than 2% was evident for all samples and compounded with repeated thermal cycling (**Supplementary Figure 4**). Polydomain LCEs demonstrated negligible actuation behavior when heated into

the isotropic regime (not shown), although a phase change from the opaque white nematic phase to the optically clear isotropic phase was obvious.

3.5 Wide angle X-ray scattering

WAXS results showed that all LCE compositions, from 0 mol.% to 45 mol.% excess acrylate were in a nematic state when measured at $T_{reduced}$ = 0.5, which was below T_i for each composition (**Figure 9a**). The nematic order was retained in the LCEs while the amount of excess acrylate concentration in the networks was varied. This is illustrated by the diffraction patterns revealing two bright spots separated by 180°, which is associated with nematic order. All LCE compositions became isotropic when heated to $T_{reduced}$ = 1.25, represented by a diffuse halo pattern (**Figure 9b**). These results help verify the T_i found by DMA testing. The 2 mol.%, 5 mol.%, and 45 mol.% had reduced intensity compared to the other samples due to the thickness of the samples tested.

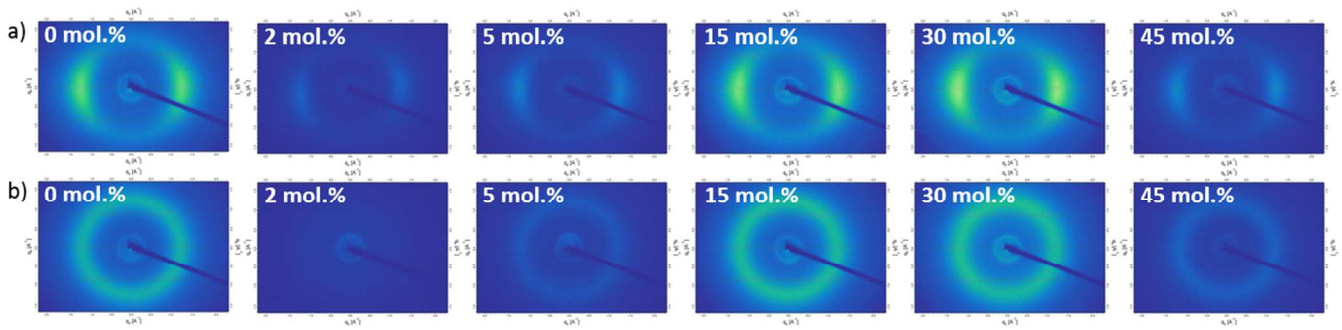

Figure 9: 2D images of WAXS (a) at $T_{reduced}$ = 0.5 demonstrated the nematic phase. The 0 mol.% sample was strained to clearing while the remaining compositions were not constrained. The mesogens in all compositions were in a nematic state. (b) $T_{reduced}$ = 1.25 demonstrating the isotropic phase.

4. Discussion

The purpose of this study was to investigate the thermomechanical and actuation behavior of monodomain nematic main-chain LCEs produced by the two-stage thiol-acrylate procedure. The nature of this reaction scheme requires an excess amount of acrylate to fix the monodomain conformation by the photochemical reaction in the second stage; however, no previous study has quantified how the amount of excess acrylate

influences fixity, thermomechanical properties, or actuation performance. Intuitively, one would expect increasing excess acrylate above 0 mol.% would increasingly improve fixity of the monodomain and reduce actuation performance due increased bonding in the second stage. Yet, the results of this study show several variables have disproportionate influence on thermomechanical behavior.

The polydomain LCEs produced by the initial Michael addition reaction were required to withstand mechanical load throughout the polydomain-monodomain transition and subsequent photochemical reaction. To facilitate this requirement, an isotropic genesis technique was used in which Michael addition was carried out in the presence of a solvent (toluene), forcing the isotropic phase throughout the duration of the Michael addition reaction. The polydomain nematic phase formed only after removing solvent by forced evaporation. It was previously shown by several studies that polydomain LCEs synthesized in the isotropic phase, referred to as iPNEs in the literature (Traugutt et al. 2017) require relatively small amount of work to complete a mechanically-induced polydomain-monodomain transition, whereas a similar transition in LCEs synthesized in the nematic phase, commonly referred to as nPNEs, is significantly more demanding (Higaki, Urayama, and Takigawa 2012; Urayama et al. 2009; Traugutt et al. 2017). Thus, it is doubtful that some of the compositions included in this study could survive the mechanical demands of the polydomain-monodomain transition if the nematic polymerization technique were used; however, employing a nematic genesis approach could further stabilize the nematic phase, resulting in greater increase T_i with acrylate content or could result in paranematic behavior. This study showed that a change in excess acrylate concentration did not affect the nematic phase of the networks, unlike a previous study which showed a change in structure, specifically spacer length, could switch the networks from nematic to smectic (Saed, Volpe, et al. 2017).

The mechanical properties of compositions with excess acrylate were relatively poor prior to the second-stage photochemical reaction. The introduction of excess acrylate produced ‘dangling ends’ within the network, which resulted in fewer covalent bonds throughout the network. Consequently, mechanical properties were

diminished, and coupling between deformation and mesogen alignment was reduced. Therefore, the applied strain required to complete the polydomain-monodomain transition increased from 85% strain for the 2 mol.% composition to 128% strain for the 45 mol.% composition (**Figure 3a**).

Surprisingly, varying excess acrylate had very little effect on monodomain programming, which was measured by fixity (**Figure 3b**). Increasing excess acrylate content from 0 mol.% to 2 mol.% increased fixity from 0% to approximately 85% due to the introduction of photochemical bonds in the 2 mol.% composition. Increasing excess acrylate content beyond 2 mol.%, which was consistent with an increase in the number of bonds formed in the photochemical reaction, did not improve fixity indicating that relatively few bonds were required to maintain the monodomain conformation. In contrast, the increase in bonds stabilized the nematic phase (Warner and Terentjev 2007; Melchert et al. 2012) and increased T_i by 55°C with increasing acrylate content, increasing T_i from 58°C to 113°C as excess acrylate increased from 0 mol.% to 45 mol.% (**Figure 4**).

Increasing acrylate content also modified molecular regularity along the network main-chain. A stoichiometric balance of thiol and acrylate groups (0 mol.%) resulted in regularly alternating mesogenic network components and spacers along the main-chain with relatively few crosslinks (originating from tetrathiol monomer) dispersed throughout the network. Increasing excess acrylate content displaced spacers with direct links between mesogenic components, which decreased the mobility of the network (Donald, Windle, and Hanna 2006; Farren et al. 2001). This increased T_g from 2°C to 14°C as acrylate increased from 0 mol.% to 45 mol.% (**Figure 4**), which compares to a previous study The disproportionate increase in T_g relative to T_i broadened the rubbery nematic regime by 44°C. Since E' was invariable in each thermal regime with respect to composition, varying excess acrylate content provides a technique to tailor T_i and/or dynamic properties without requiring a change of monomers or synthetic approach.

Damping properties in the rubbery nematic regime decreased with increasing acrylate (**Figure 5**). Low acrylate compositions demonstrated elevated *tan δ* (**Figure 5b**), suggesting relatively high mesogen mobility and moderate damping properties; however, the increase of stabilizing bonds in high acrylate compositions decreased damping performance severely. The dynamic soft elastic dip in *E'* at T_i (**Figure 5a**) became less dramatic and broadened with increasing acrylate content as mesogen mobility became more restricted by the increasing number of photochemical bonds. This was coincident with the *tan δ* peak at T_i that was present in low acrylate compositions but vanished with increasing acrylate content. This is suggestive of paranematic behavior in high acrylate compositions; however, paranematicism is typically associated with an absence of dynamic soft elasticity and T_i that is difficult or impossible to detect by thermomechanical techniques (Lebar et al. 2012; Traugutt et al. 2017; Kim et al. 2017; Domenici 2012). Rather, increased inhomogeneity along the main-chain with increasing acrylate content is more likely to be responsible for broadening the isotropic transition. The WAXS results at $T_{reduced}$ = 1.25 (**Figure 9a**) did not indicate paranematic behavior for any composition at that temperature.

E' in the isotropic phase did not vary significantly with composition (**Figure 5a**). As with isotropic rubbers, LCEs in the isotropic regime show strong dependence of *E'* on crosslink density (Martella et al. 2015; Burke and Mather 2010). The uniformity of *E'* between compositions in this study suggests negligible branching of acrylate groups during the photochemical reaction. Thus, the crosslink density was dictated by the tetrathiol crosslinking monomer.

In contrast to the monodomain conformation, the polydomain composition (0 mol.%) maintained lower *E'* over the entire temperature range tested (**Figure 6a**) and an elevated *tan δ* within the rubbery nematic regime (**Figure 6b**). These observations are consistent with the relatively high mobility of individual domains throughout the polydomain conformation, indicating superior damping properties. The 15 mol.% polydomain demonstrated trends in *E'* and *tan δ* similar to the 0 mol.% composition with the exception of significantly

reduced damping throughout the rubbery nematic regime as a result of the greater number of bonds fixing the nematic phase and an associated limitation on domain mobility.

Tensile testing at $T_{reduced}$ = 0.55 demonstrated mechanical properties of the rubbery nematic regime at temperatures well above the glass transition for each composition. The linear responses parallel the director were consistent with traditional elastomeric extension of main-chain spacers and showed no evidence of mesogen rotation (**Figure 7a**). Thus, permanent deformation was negligible after loading to high strain (**Figure 7b**). This suggests a high degree of order was achieved by the fixing reaction, which agrees with the fixity results. The increase of $E_{//}$ with acrylate content from 1.4 MPa to 6.1 MPa was consistent with a reduction of flexible spacers along the main-chain and resulted in reduction of main-chain extensibility. Godman, et al (Godman et al. 2017) observed a similar trend in E parallel to the director in monodomain thiol-acrylate LCEs with varied main-chain length between mesogens. The broad plateau that developed in response to tensile loading perpendicular to the director (**Figure 7c**) agrees with classic soft elasticity exhibited during widespread mesogen rotation. This deformation mechanism produced distinct necking, which spread throughout the gauge length of each sample (**Figure 7d**). All monodomain compositions demonstrated the same characteristic plateau with variation in $E_{\perp}$ and σ_{th}. Similar to the parallel response to loading, $E_{\perp}$ increased from 0.6 MPa to 2.6 MPa with acrylate content due to changes in main-chain composition. σ_{th} also increased from 14 kPa to 208 kPa as a result of the increase in bonds stabilizing mesogen alignment, although this trend was difficult to detect in low acrylate compositions.

Monodomain composition had little influence on the total actuation strain (**Figure 8a**), which ranged from 84% to 90%, despite the increase in photochemical bonds with increasing acrylate. Thus, changing acrylate content allowed selectivity of the actuation temperature (T_i) without sacrificing actuation strain. The increase in photochemical bonds stabilizing the nematic phase produced a decrease in actuation rate near T_i from 10.8%/°C to 1.8%/°C as excess acrylate increased from 2 mol.% to 45 mol.% (**Figure 8b**). The 2 mol.% composition,

which had the fewest stabilizing bonds, showed actuation behavior approaching a discontinuous phase transition characterized by a jump in strain as the LCE transitioned between nematic and isotropic phases (Lebar et al. 2012). On the other hand, the high acrylate compositions demonstrated gradual change in strain through the transition with significant actuation in the isotropic regime, which agrees with the broad isotropic transition shown by DMA.

5. Conclusions

This study investigated the influence of acrylate content on thermomechanical properties of monodomain main-chain LCEs. The results demonstrate a technique to tune the thermal regimes without influencing total actuation strain or dynamic mechanical properties within each regime. Photochemical reaction of excess acrylate in the nematic monodomain conformation programmed the monodomain with greater than 85% fixity for all compositions. Increasing acrylate content resulted in more bonding during the photochemical reaction, which produced an increasingly more stable nematic phase. Consequently, T_i increased from 58°C to 113°C with an increase in excess acrylate from 2 mol.% to 45 mol.% and broadened the rubbery nematic regime by 44°C. *E'* was invariant with composition in each thermal regime but the increase in photochemical bonding with acrylate content influenced dynamic soft elasticity at T_i. Low acrylate compositions demonstrated narrow transitions to the isotropic phase with dramatic decreases in *E'* and peaks in *tan* δ resulting from high mesogen mobility. On the other hand, high acrylate compositions exhibited broader transitions without enhanced damping owing to the greater number of photochemical bonds and reduced mesogen mobility. Tensile mechanical properties perpendicular to the director demonstrated in increase in σ_{th} from 14 kPa to 208 kPa with excess acrylate owing to increased number of bonds fixing the monodomain. $E_{/\!/}$ and $E_{\perp}$, measured during the initial tensile loading parallel and perpendicular to the director, respectively, increased from 1.4 MPa to 6.1 MPa and from 0.6 MPa to 2.6 MPa with excess acrylate due to structural changes along the main-chain. Total strain actuation did not vary significantly with composition, ranging between 84% and 90% along the director. Actuation rate at T_i decreased

against excess acrylate content, decreasing from 10.8% strain/°C for 2 mol.% excess acrylate to 1.8% strain/°C for 30 mol.% and 45 mol.% excess acrylate owing to the increase in photochemical bonds.

Supporting Information:

SupportingFigures.pdf

Author Contributions

The manuscript was written through contributions of all authors. All authors have given approval to the final version of the manuscript.

Funding Sources

C.P.F. appreciates support from an Institutional Development Award (IDeA) from the National Institute of General Medical Sciences of the National Institutes of Health under Grant No. 2P20GM103432. C.M.Y. thanks the National Science Foundation Faculty Early Career Development Program.

Acknowledgment

The authors thank Mohand Saed for his guidance and Viren Patel for his contribution to experimental work.

6. References

Ahn, Chihyung, Xudong Liang, and Shengqiang Cai. 2015. "Inhomogeneous Stretch Induced Patterning of Molecular Orientation in Liquid Crystal Elastomers." *Extreme Mechanics Letters* 5. Elsevier Ltd: 30–36. doi:10.1016/j.eml.2015.09.007.

Ambulo, Cedric P., Julia J. Burroughs, Jennifer M. Boothby, Hyun Kim, M. Ravi Shankar, and Taylor H. Ware. 2017. "Four-Dimensional Printing of Liquid Crystal Elastomers." *ACS Applied Materials and Interfaces* 9 (42): 37332–39. doi:10.1021/acsami.7b11851.

Babakhanova, Greta, Taras Turiv, Yubing Guo, Matthew Hendrikx, Qi-Huo Wei, Albert P H J Schenning, Dirk J Broer, and Oleg D Lavrentovich. 2018. "Liquid Crystal Elastomer Coatings with Programmed Response of Surface Profile." *Nature Communications* 9 (1). Springer US: 456. doi:10.1038/s41467-018-02895-9.

Bera, Tanmay, Ernest J. Freeman, Jennifer A. McDonough, Robert J. Clements, Asaad Aladlaan, Donald W. Miller, Christopher Malcuit, Torsten Hegmann, and Elda Hegmann. 2015. "Liquid Crystal Elastomer Microspheres as Three-Dimensional Cell Scaffolds Supporting the Attachment and Proliferation of Myoblasts." *ACS Applied Materials & Interfaces* 7 (26). American Chemical Society: 14528–35. doi:10.1021/acsami.5b04208.

Boothby, Jennifer M., Hyun Kim, and Taylor H. Ware. 2017. "Shape Changes in Chemoresponsive Liquid Crystal Elastomers." *Sensors and Actuators B: Chemical* 240. Elsevier B.V.: 511–18. doi:10.1016/j.snb.2016.09.004.

Burke, Kelly a., and Patrick T. Mather. 2010. "Soft Shape Memory in Main-Chain Liquid Crystalline Elastomers." *Journal of Materials Chemistry* 20 (17): 3449. doi:10.1039/b924050k.

Dey, Sonal, Dena Agra-Kooijman, Wanting Ren, Philip McMullan, Anselm Griffin, and Satyendra Kumar. 2013. "Soft Elasticity in Main Chain Liquid Crystal Elastomers." *Crystals* 3 (2): 363–90. doi:10.3390/cryst3020363.

Domenici, Valentina. 2012. "2H NMR Studies of Liquid Crystal Elastomers: Macroscopic vs. Molecular Properties." *Progress in Nuclear Magnetic Resonance Spectroscopy* 63. Elsevier B.V.: 1–32. doi:10.1016/j.pnmrs.2011.07.003.

Donald, A.M. (University of Cambridge), A. H. (University of Cambridge) Windle, and S. (University of Bristol) Hanna. 2006. *Liquid Crystalline Polymers*. 2nded. Cambridge University Press.

Donnio, Bertrand, Hendrik Wermter, and Heino Finkelmann. 2000. "A Simple and Versatile Synthetic Route for the Preparation of Main-Chain, Liquid-Crystalline Elastomers." *Macromolecules* 33 (21). American Chemical Society: 7724–29. doi:10.1021/ma0002850.

Farren, C, M Akatsuka, Y Takezawa, and Y Itoh. 2001. "Thermal and Mechanical Properties of Liquid Crystalline Epoxy Resins as a Function of Mesogen Concentration" 42: 1507–14.

Fleischmann, Eva-Kristina, F. Romina Forst, Katrin Köder, Nadia Kapernaum, and Rudolf Zentel. 2013. "Microactuators from a Main-Chain Liquid Crystalline Elastomer via Thiol–ene 'click' Chemistry." *Journal of Materials Chemistry C* 1 (37): 5885. doi:10.1039/c3tc30272e.

Frick, Carl P., Daniel R. Merkel, Christopher M. Laursen, Stephan A. Brinckmann, and Christopher M. Yakacki. 2016. "Copper-Coated Liquid-Crystalline Elastomer via Bioinspired Polydopamine Adhesion and Electroless Deposition." *Macromolecular Rapid Communications* 37 (23): 1912–17. doi:10.1002/marc.201600363.

Gao, Yunxiang, Taizo Mori, Sarah Manning, Yu Zhao, Alek D. Nielsen, Abdollah Neshat, Anshul Sharma, et al. 2016. "Biocompatible 3D Liquid Crystal Elastomer Cell Scaffolds and Foams with Primary and Secondary Porous Architecture." *ACS Macro Letters* 5 (1): 4–9. doi:10.1021/acsmacrolett.5b00729.

Gelebart, Anne Helene, Matthew Mc Bride, Albertus P H J Schenning, Christopher N. Bowman, and Dirk J. Broer. 2016. "Photoresponsive Fiber Array: Toward Mimicking the Collective Motion of Cilia for Transport Applications." *Advanced Functional Materials* 26 (29): 5322–27. doi:10.1002/adfm.201601221.

Giamberini, Marta, Pierfrancesco Cerruti, Veronica Ambrogi, Cosimo Vestito, Francesco Covino, and Cosimo Carfagna. 2005. "Liquid Crystalline Elastomers Based on Diglycidyl Terminated Rigid Monomers and Aliphatic Acids. Part 2. Mechanical Characterization." *Polymer* 46 (21): 9113–25. doi:10.1016/j.polymer.2005.04.093.

Godman, Nicholas P., Benjamin A. Kowalski, Anesia D. Auguste, Hilmar Koerner, and Timothy J. White. 2017. "Synthesis of Elastomeric Liquid Crystalline Polymer Networks via Chain Transfer." *ACS Macro Letters* 6 (11): 1290–95. doi:10.1021/acsmacrolett.7b00822.

Hanzon, Drew W., Nicholas A. Traugutt, Matthew K. McBride, Christopher N. Bowman, Christopher M. Yakacki, and Kai Yu. 2018. "Adaptable Liquid Crystal Elastomers with Transesterification-Based Bond Exchange Reactions." *Soft Matter*. Royal Society of Chemistry. doi:10.1039/C7SM02110K.

Hessberger, Tristan, Lukas Braun, and Rudolf Zentel. 2016. "Microfluidic Synthesis of Actuating Microparticles from a Thiol-Ene Based Main-Chain Liquid Crystalline Elastomer." *Polymers* 8 (12). doi:10.3390/polym8120410.

Higaki, Haruko, Kenji Urayama, and Toshikazu Takigawa. 2012. "Memory and Development of Textures of Polydomain Nematic Elastomers." *Macromolecular Chemistry and Physics* 213 (18): 1907–12. doi:10.1002/macp.201200239.

Hong, Yang, Axel Buguin, Jean Marie Taulemesse, Kosuke Kaneko, Stéphane Méry, Anne Bergeret, and Patrick Keller. 2009. "Micron-Sized Main-Chain Liquid Crystalline Elastomer Actuators with Ultralarge Amplitude Contractions." *Journal of the American Chemical Society* 131 (41): 15000–4. doi:10.1021/ja905363f.

Hoyle, Charles E, and Christopher N Bowman. 2010. "Thiol-Ene Click Chemistry." *Angewandte Chemie (International Ed. in English)* 49 (9): 1540–73. doi:10.1002/anie.200903924.

Kim, Hyun, Jennifer M. Boothby, Sarvesh Ramachandran, Cameron D. Lee, and Taylor H. Ware. 2017.

"Tough, Shape-Changing Materials: Crystallized Liquid Crystal Elastomers." *Macromolecules*, acs.macromol.7b00567. doi:10.1021/acs.macromol.7b00567.

Kotikian, Arda, Ryan L. Truby, John William Boley, Timothy J. White, and Jennifer A. Lewis. 2018. "3D Printing of Liquid Crystal Elastomeric Actuators with Spatially Programed Nematic Order." *Advanced Materials* 1706164: 1706164. doi:10.1002/adma.201706164.

Kowalski, Benjamin A., Tyler C. Guin, Anesia D. Auguste, Nicholas P. Godman, and Timothy J. White. 2017. "Pixelated Polymers: Directed Self Assembly of Liquid Crystalline Polymer Networks." *ACS Macro Letters* 6 (4): 436–41. doi:10.1021/acsmacrolett.7b00116.

Kowalski, Benjamin A., Vincent P. Tondiglia, Tyler Guin, and Timothy J. White. 2017. "Voxel Resolution in the Directed Self-Assembly of Liquid Crystal Polymer Networks and Elastomers." *Soft Matter* 13 (24): 4335–40. doi:10.1039/C7SM00663B.

Kragt, Augustinus J.J., Dirk J. Broer, and Albertus P.H.J. Schenning. 2018. "Easily Processable and Programmable Responsive Semi-Interpenetrating Liquid Crystalline Polymer Network Coatings with Changing Reflectivities and Surface Topographies." *Advanced Functional Materials* 28 (6): 1–7. doi:10.1002/adfm.201704756.

Krause, Simon, Frank Zander, Gerd Bergmann, Holger Brandt, Hendrik Wertmer, and Heino Finkelmann. 2009. "Nematic Main-Chain Elastomers: Coupling and Orientational Behavior." *Comptes Rendus Chimie* 12 (1–2). Elsevier Masson SAS: 85–104. doi:10.1016/j.crci.2008.08.003.

Kularatne, Ruvini S., Hyun Kim, Jennifer M. Boothby, and Taylor H. Ware. 2017. "Liquid Crystal Elastomer Actuators: Synthesis, Alignment, and Applications." *Journal of Polymer Science Part B: Polymer Physics* 55 (5): 395–411. doi:10.1002/polb.24287.

Küpfer, Jürgen, and Heino Finkelmann. 1991. "Nematic Liquid Single Crystal Elastomers." *Die Makromolekulare Chemie, Rapid Communications* 12 (12). Hüthig & Wepf Verlag: 717–26.

doi:10.1002/marc.1991.030121211.

Lebar, Andrija, George Cordoyiannis, Zdravko Kutnjak, and Boštjan Zalar. 2012. “The Isotropic-to-Nematic Conversion in Liquid Crystalline Elastomers.” In *Liquid Crystalline Elastomers: Materials and Applications*, edited by W. H. de Jeu, 147–85. Springer. http://link.springer.com/10.1007/12_2010_103.

Liu, Li, Mei Hua Liu, Lin Lin Deng, Bao Ping Lin, and Hong Yang. 2017. “Near-Infrared Chromophore Functionalized Soft Actuator with Ultrafast Photoresponsive Speed and Superior Mechanical Property.” *Journal of the American Chemical Society* 139 (33): 11333–36. doi:10.1021/jacs.7b06410.

Martella, Daniele, Camilla Parmeggiani, Diederik Sybolt Wiersma, Milagros Piñol, and Luis Oriol. 2015. “The First Thiol–yne Click Chemistry Approach for the Preparation of Liquid Crystalline Elastomers.” *J. Mater. Chem. C* 3 (34). Royal Society of Chemistry: 9003–10. doi:10.1039/C5TC01290B.

McBride, Matthew K., Matthew Hendrikx, Danqing Liu, Brady T. Worrell, Dirk J. Broer, and Christopher N. Bowman. 2017. “Photoinduced Plasticity in Cross-Linked Liquid Crystalline Networks.” *Advanced Materials* 29 (17). doi:10.1002/adma.201606509.

Melchert, Christian, Marc Behl, Ulrich Nöchel, and Andreas Lendlein. 2012. “Influence of Comesogens on the Thermal and Actuation Properties of 2-Tert-Butyl-1,4-bis[4-(4-Pentenyloxy)benzoyl]hydroquinone Based Nematic Main-Chain Liquid Crystalline Elastomers.” *Macromolecular Materials and Engineering* 297 (12): 1203–12. doi:10.1002/mame.201200238.

Mostajeran, Cyrus, Taylor H. Ware, and Timothy J. White. 2015. “Encoding Gaussian Curvature in Glassy and Elastomeric Liquid Crystal Polymer Networks.” doi:10.1098/rspa.2016.0112.

Nair, D.P., Neil B Cramer, John C Gaipa, Matthew K McBride, Emily M Matherly, Robert R McLeod, Robin Shandas, and Christopher N Bowman. 2012. “Two-Stage Reactive Polymer Network Forming Systems.” *Advanced Functional Materials* 22 (7). WILEY-VCH Verlag: 1502–10. doi:10.1002/adfm.201102742.

Nair, D.P., Maciej Podgórski, Shunsuke Chatani, Tao Gong, Weixian Xi, Christopher R. Fenoli, and Christopher N. Bowman. 2014. "The Thiol-Michael Addition Click Reaction: A Powerful and Widely Used Tool in Materials Chemistry." *Chemistry of Materials* 26 (1). American Chemical Society: 724–44. doi:10.1021/cm402180t.

Ohm, Christian, Martin Brehmer, and Rudolf Zentel. 2010. "Liquid Crystalline Elastomers as Actuators and Sensors." *Advanced Materials* 22 (31): 3366–87. doi:10.1002/adma.200904059.

Pei, Zhiqiang, Yang Yang, Qiaomei Chen, Eugene M Terentjev, Yen Wei, and Yan Ji. 2014. "Mouldable Liquid-Crystalline Elastomer Actuators with Exchangeable Covalent Bonds." *Nature Materials* 13 (1). Nature Publishing Group: 36–41. doi:10.1038/nmat3812.

Petridis, L., and E. M. Terentjev. 2006. "Nematic-Isotropic Transition with Quenched Disorder." *Physical Review E - Statistical, Nonlinear, and Soft Matter Physics* 74 (5): 1–11. doi:10.1103/PhysRevE.74.051707.

Prévôt, Marianne, Senay Ustunel, and Elda Hegmann. 2018. "Liquid Crystal Elastomers—A Path to Biocompatible and Biodegradable 3D-LCE Scaffolds for Tissue Regeneration." *Materials* 11 (3): 377. doi:10.3390/ma11030377.

Saed, Mohand O., Amir H. Torbati, D.P. Nair, and Christopher M. Yakacki. 2016. "Synthesis of Programmable Main-Chain Liquid-Crystalline Elastomers Using a Two-Stage Thiol-Acrylate Reaction." *Journal of Visualized Experiments*, no. 107(January). doi:10.3791/53546.

Saed, Mohand O., Amir H. Torbati, Chelsea A. Starr, Rayshan Visvanathan, Noel A. Clark, and Christopher M. Yakacki. 2017. "Thiol-Acrylate Main-Chain Liquid-Crystalline Elastomers with Tunable Thermomechanical Properties and Actuation Strain." *Journal of Polymer Science Part B: Polymer Physics* 55 (2): 157–68. doi:10.1002/polb.24249.

Saed, Mohand O., Ross H. Volpe, Nicholas A. Traugutt, Rayshan Visvanathan, Noel A. Clark, and Christopher M. Yakacki. 2017. "High Strain Actuation Liquid Crystal Elastomers via Modulation of Mesophase

Structure." *Soft Matter* 13. Royal Society of Chemistry: 7537–47. doi:10.1039/C7SM01380A.

Sánchez-Ferrer, Antoni, and Heino Finkelmann. 2010. "Thermal and Mechanical Properties of New Main-Chain Liquid-Crystalline Elastomers." *Solid State Sciences* 12 (11): 1849–52. doi:10.1016/j.solidstatesciences.2010.01.017.

Schuhladen, Stefan, Falko Preller, Richard Rix, Sebastian Petsch, Rudolf Zentel, and Hans Zappe. 2014. "Iris-like Tunable Aperture Employing Liquid-Crystal Elastomers." *Advanced Materials (Deerfield Beach, Fla.)* 26 (42): 7247–51. doi:10.1002/adma.201402878.

Torras, Núria, Kirill E. Zinoviev, Jaume Esteve, and Antoni Sánchez-Ferrer. 2013. "Liquid-Crystalline Elastomer Micropillar Array for Haptic Actuation." *Journal of Materials Chemistry C* 1 (34): 5183. doi:10.1039/c3tc31109k.

Traugutt, N. A., R. H. Volpe, M. S. Bollinger, M.O. Saed, A. H. Torbati, K. Yu, Natalia Dadivanyan, and C.M. Yakacki. 2017. "Liquid-Crystal Order during Synthesis Affects Main-Chain Liquid-Crystal Elastomer Behavior." *Soft Matter*. doi:10.1039/C7SM01405H.

Urayama, Kenji, Etsuko Kohmon, Masahiro Kojima, and Toshikazu Takigawa. 2009. "Polydomain−Monodomain Transition of Randomly Disordered Nematic Elastomers with Different Cross-Linking Histories." *Macromolecules* 42 (12): 4084–89. doi:10.1021/ma9004692.

Urbanski, Martin, Catherine G. Reyes, Junghyun Noh, Anshul Sharma, Yong Geng, Venkata Subba Rao Jampani, Jan P.F. F Lagerwall, Venkata Subba Rao Jampani, and Jan P.F. F Lagerwall. 2017. "Liquid Crystals in Micron-Scale Droplets, Shells and Fibers." *Journal of Physics: Condensed Matter* 29 (13). IOP Publishing. doi:10.1088/1361-648X/aa5706.

Wang, Li, Wei Liu, Ling-Xiang Guo, Bao-Ping Lin, Xue-Qin Zhang, Ying Sun, and Hong Yang. 2017. "A Room-Temperature Two-Stage Thiol–ene Photoaddition Approach towards Monodomain Liquid Crystalline Elastomers." *Polym. Chem.* 8 (8). Royal Society of Chemistry: 1364–70.

doi:10.1039/C6PY02096H.

Wang, Meng, Bao Ping Lin, and Hong Yang. 2016. “A Plant Tendril Mimic Soft Actuator with Phototunable Bending and Chiral Twisting Motion Modes.” *Nature Communications* 7. Nature Publishing Group: 1–8. doi:10.1038/ncomms13981.

Wang, Meng, Sayed Mir Sayed, Ling Xiang Guo, Bao Ping Lin, Xue Qin Zhang, Ying Sun, and Hong Yang. 2016. “Multi-Stimuli Responsive Carbon Nanotube Incorporated Polysiloxane Azobenzene Liquid Crystalline Elastomer Composites.” *Macromolecules* 49 (2): 663–71. doi:10.1021/acs.macromol.5b02388.

Wang, Zhijian, Hongmiao Tian, Qiguang He, and Shengqiang Cai. 2017. “Reprogrammable, Reprocessible, and Self-Healable Liquid Crystal Elastomer with Exchangeable Disulfide Bonds.” *ACS Applied Materials & Interfaces* 9 (38): 33119–28. doi:10.1021/acsami.7b09246.

Ware, T. H., M. E. McConney, J. J. Wie, V. P. Tondiglia, and T.J. White. 2015. “Voxelated Liquid Crystal Elastomers.” *Science* 347 (6225): 982–84. doi:10.1126/science.1261019.

Ware, T.H., John S Biggins, Andreas F Shick, Mark Warner, and T.J. White. 2016. “Localized Soft Elasticity in Liquid Crystal Elastomers.” *Nature Communications* 7. Nature Publishing Group: 10781. doi:10.1038/ncomms10781.

Warner, M., and E.M. Terentjev. 2007. *Liquid Crystal Elastomers*. Oxford University Press.

Wermter, Hendrik, and Heino Finkelmann. 2001. “Liquid Crystalline Elastomers as Artificial Muscles.” *E-Polymers* 1 (1): 111–23. doi:10.1515/epoly.2001.1.1.111.

White, T.J. 2018. “Photomechanical Effects in Liquid Crystalline Polymer Networks and Elastomers.” *Journal of Polymer Science Part B: Polymer Physics*, January, 1–11. doi:10.1002/polb.24576.

White, T.J., and D.J. Broer. 2015. “Programmable and Adaptive Mechanics with Liquid Crystal Polymer Networks and Elastomers.” *Nature Materials* 14 (11). Nature Publishing Group, a division of Macmillan

Publishers Limited. All Rights Reserved.: 1087–98. doi:10.1038/nmat4433.

Yakacki, C.M., M.O. Saed, D.P. Nair, T. Gong, S.M. Reed, and C.N. Bowman. 2015. "Tailorable and Programmable Liquid-Crystalline Elastomers Using a Two-Stage Thiol–acrylate Reaction." *RSC Adv.* 5 (25). The Royal Society of Chemistry: 18997–1. doi:10.1039/C5RA01039J.

Yang, Hong, Ming Xia Liu, Yue Wei Yao, Ping Yang Tao, Bao Ping Lin, Patrick Keller, Xue Qin Zhang, Ying Sun, and Ling Xiang Guo. 2013. "Polysiloxane-Based Liquid Crystalline Polymers and Elastomers Prepared by Thiol-Ene Chemistry." *Macromolecules* 46 (9): 3406–16. doi:10.1021/ma400462e.

Yuan, Chao, Devin J. Roach, Conner K. Dunn, Quanyi Mu, Xiao Kuang, Christopher M. Yakacki, T. J. Wang, Kai Yu, and H. Jerry Qi. 2017. "3D Printed Reversible Shape Changing Soft Actuators Assisted by Liquid Crystal Elastomers." *Soft Matter* 13. Royal Society of Chemistry: 5558–68. doi:10.1039/C7SM00759K.

For table of contents use only

Thermomechanical Properties of Monodomain Nematic Main-Chain Liquid Crystal Elastomers

Daniel R. Merkel[1], *Nick Traugutt*[2], *Rayshan Visvanathan*[3], *Christopher M. Yakacki*[2], *and Carl P. Frick*[1λ]

Actuation temperature was controlled without influencing total actuation performance in liquid crystal elastomers fabricated by a two-stage reaction scheme.